Kohmaru *et al. Journal of Cardiothoracic Surgery* (2024) 19:645
https://doi.org/10.1186/s13019-024-03182-z

Journal of Cardiothoracic Surgery

RESEARCH **Open Access**

Intraoperative patient radiation dose from cone-beam computed tomography in thoracic surgery

Shinya Kohmaru[1], Yuichi Saito[1*], Takeshi Takata[2], Shizuka Morita[1], Ryo Takeyama[1], Yasuyuki Kanamoto[1], Tomoki Nishida[1], Hitoshi Dejima[1], Yoshikane Yamauchi[1], Ikuo Kobayashi[3], Masafumi Kawamura[4] and Yukinori Sakao[1]

Abstract

Background Several methods can be used to intraoperatively identify pulmonary lesion using radiation technology. However, little is known about patient radiation exposure during chest surgery. We aimed to measure patients' radiation exposure from cone-beam computed tomography (CBCT) used in a hybrid operating room.

Methods This retrospective study included patients who underwent surgical treatment in a hybrid operating room between April 2019 and December 2023 at the Teikyo University Hospital. All data was obtained prospectively, but the study was approved by the IRB as a retrospective study because of repeated extensions of study period in order to collect more cases. Skin radiation exposure was measured using five wearable dosimeters per patient. The measurements were compared to cumulative Air Kerma. Furthermore, the radiation exposure dose on the surgical side, which cannot be measured, was estimated by computer simulation.

Results Among 182 patients who underwent surgery in a hybrid operating room, radiation exposure measurements were conducted on 67 patients. The patients' mean age was 60.7 years. The average number of CBCT scans was 2.1 (1–5) and the intraoperative identification rate was 100%, with no marking-related complications. Average patient's skin radiation dose was 3.69 ± 5.48 mGy per dosimeter, and cumulative Air Kerma was 25.4 ± 19.3 mGy. The highest radiation exposure was recorded in the 5th intercostal space whereas the lowest was measured in the supraclavicular or 11th intercostal spaces. Referring to phantom and computer simulation data, the 5th and 8th intercostal spaces were significantly more exposed to radiation at not only measurement side but also the surgical field, particularly when the number of CT scans was four.

Conclusion We found that the patient's 5th to 8th intercostal space was the most radiation exposed area by intraoperative CBCT imaging because the CBCT movement was restricted by the patient's arm, anesthesia machine, and operating table during chest surgery. In future, it is strongly required to research for radiation protection in

Meeting Presentation: The 32nd international congress of the European Association for Endoscopic Surgery.

*Correspondence:
Yuichi Saito
k3699004@gmail.com
Full list of author information is available at the end of the article

this area. Furthermore, performing no more than three scans intraoperatively may be preferable in order to protect patients from radiation exposure during CBCT guided thoracic surgery.

Keywords Cone-beam computed tomography, Navigation surgery, Radiation exposure, Small lung cancer, Video-assisted thoracoscopic surgery

Background

Lung cancer is the leading cause of cancer-related death, accounting for 1.79 million deaths (18.0% of total cancer deaths) and the most frequent cancer, accounting for 2.20 million new cases according to GLOBOCAN 2020 [1]. In 2011, the National Lung Screening Trial demonstrated a 20% reduction in lung cancer mortality with three annual low-dose computed tomography (CT) screenings for patients at a high risk of lung cancer in the United States. Furthermore, in 2020, the Nederlands-Leuvens Longkanker Screenings Onderzoek trial reported that the 10-year lung cancer mortality in high-risk patients was significantly lower in the CT-screening cohort than in the no-screening cohort [2, 3]. Accordingly, some guidelines recommend screening using low-dose CT for patients at risk of lung cancer [4, 5]. This increase in the number of CT examinations resulted in the increased detection rate of small pulmonary nodules, which poses a new challenge to thoracic surgeons regarding how to intraoperatively identify very small lesions [6, 7].

Previously, small pulmonary nodules were identified by the surgeon's direct touch during thoracotomy, and surgery was not indicated if the pulmonary nodules were too small to palpate. Thereafter, when video-assisted thoracic surgery became common, the small surgical incision made it difficult for thoracic surgeons to palpate small pulmonary nodules intraoperatively. Therefore, novel intraoperative identification methods have been developed one after another to replace the tactile methods. CT-guided marking was first developed for the intraoperative localization of small peripheral pulmonary nodules [8, 9]. In the early 1990s, percutaneous needle localization using metal hook-wire placement was developed and rapidly spread. However, serious complications such as dislodging and migration of the wire, air embolism, bleeding and pneumothorax were reported [10, 11]. Some researchers then started using dyes as markers instead of metals to reduce fatal complications; however, some minor complications in percutaneous dye marking were reported [12–14]. Moreover, the dye marker eventually disappears, making intraoperative identification difficult [15].

In 1997, Kobayashi et al. reported CT-guided bronchoscopic barium marking, which overcame some of the disadvantages of percutaneous needle metal and/or dye marking [16]. The transbronchial approach provided a safer technique than the percutaneous approach. However, this method was not widely used at that time owing to difficulties performing a CT examination during bronchoscopy in most medical institutions. Subsequent novel technological innovations including ultrathin bronchoscopy and/or virtual bronchoscopy, brought the transbronchial approach back into the limelight [17]. In 2014, virtual-assisted lung mapping (VAL-MAP 1.0) was reported as a preoperative transbronchial multispot dye-marking technique with a good success rate for marking detection intraoperatively without causing additional complications [18]. Currently, VAL-MAP 2.0, with microcoils in the bronchus near the central stump during segmentectomy is under development [19]. Intraoperative identification using these transbronchial techniques is an excellent research-based method. However, these techniques have yet to be widely adopted in clinical practice because they require multiple highly skilled bronchoscopists and a more effective dye marker, especially in cases of severe emphysema. Additionally, there is a risk of residual microcoils in VAL-MAP 2.0.

Recently, hybrid operating rooms (ORs) equipped with cone-beam CT (CBCT) have become popular worldwide because minimally invasive treatments of cardiovascular diseases such as endovascular aortic repair (EVAR) or transcatheter aortic valve implantation (TAVI) have been recommended in the cardiovascular guidelines [20–23]. Although its popularity in general thoracic surgery has been slow, with the widespread use of EVAR or TAVI, CBCT can also be used for intraoperatively identifying nonpalpable pulmonary lesions [24–26]. These thoracoscopic marking methods using CBCT are expected to be third-generation approaches, following percutaneous needle and transbronchial approaches. The most significant feature was the absence of preoperative markings, meaning that thoracoscopic marking followed by surgery can be performed simultaneously in a hybrid OR. Moreover, there are almost no marking-related complications or psychological anxiety in patients. However, there were a few reports on the extent of the patient radiation exposure during CBCT surgery in a hybrid operating room, and the details remains unknown [27]. Therefore, it is necessary to investigate patient radiation dose in detail during thoracic surgery due to develop less invasive intraoperative identification for small peripheral pulmonary nodule. Accordingly, in this study, we aimed to measure radiation exposure dose at patient's skin level who underwent during thoracic surgery in a hybrid OR, and also conducted a measurement experiment using a phantom.

Materials and methods

Study design

This retrospective study was approved by the Institutional Review Board of the Teikyo University School of Medicine (approval number: 20–068) and conducted in accordance with the Declaration of Helsinki, as revised in 2013. We collected clinical data of patients who underwent surgical treatment in a hybrid OR between April 2019 and December 2023 at the Teikyo University Hospital from their electronic medical records. Multi-detector CT (MDCT; Aquilion ONE TSX-301C320, Toshiba, Japan) was performed on all patients preoperatively. All resected tissue specimens were obtained and pathologically diagnosed.

Inclusion and exclusion criteria

The inclusion criteria for surgery in a hybrid OR was that intraoperative localization was required to identify small pulmonary nodules, pleural lesions or chest wall mass. Conversely, we excluded cases from this study when the target lesions were expected to be easily identified during surgery (Fig. 1). Patients with simultaneous bilateral lesions were considered as ineligible cases, and patients without informed consent were unsuitable for this study. And, if data for more than 90% of the clinicopathological variables were missing, the patient was excluded from the study.

Thoracic surgery in a hybrid operating room

In our department, a hybrid OR is prepared for patients with thoracic diseases requiring intraoperative localization. This is particularly useful for patients with peripheral small pulmonary nodules that require surgical resection due to the presence of malignant features. According to our previous publication, no bronchoscopy and/or percutaneous needle puncture was needed to identify the lesions intraoperatively in a hybrid OR where CBCT (Allura Xper FD20, Phillips, The Netherlands) and a free-floating table (Maquet Co., Ltd., Germany) were available for use at any time [26]. CBCT imaging was performed during an end-inspiration breath-hold using a standard 10-s CBCT protocol to identify the target lesions. All images were taken using a standard lung protocol for CBCT, without any special optimization.

Skin dose measurement in a hybrid operating room

A wearable dosimeter (nanoDot®; Nagase Landauer, Tsukuba, Japan) was used during thoracic surgery in a hybrid OR to measure the radiation exposure of patients. It was an optically Stimulated Luminescence Dosimeter made of Aluminum Oxide, calibrated on phantom with 80kVp X-lays. In this study, the patient's

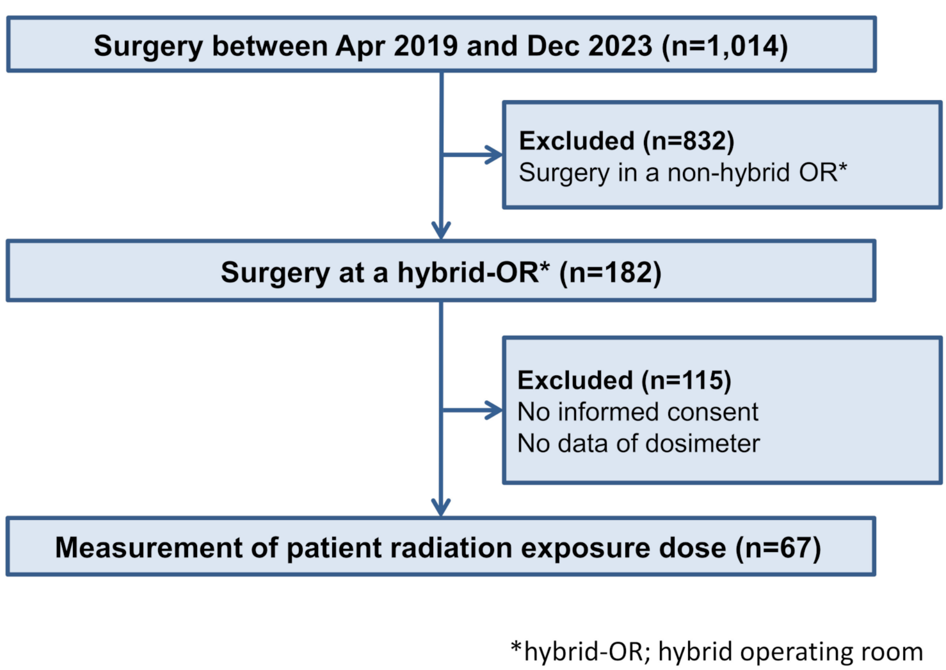

Fig. 1 Flowchart of patient enrolment into this study. After collecting data of all surgeries at Teikyo University Hospital from April 2019 to December 2013, we excluded surgical cases which were performed in a non-hybrid operating room. Finally, we enrolled patients with wearable dosimeters into this study to investigate radiation exposure from cone-beam computed tomography

skin surface dose was measured. We were able to attach the wearable dosimeters to chest wall not in surgical field which must be kept clean. Five wearable dosimeters were attached on the body surface of each patient at five locations: the fossa supraclavicularis major (FSM), second intercostal midclavicular line (2nd IC), 5th intercostal midclavicular line (5th IC), 8th intercostal midclavicular line (8th IC), and 11th intercostal midclavicular line (11th IC) (Fig. 2). After general anaesthesia with endotracheal intubation, all patients were placed on a free-floating table in the lateral position; in other words, the surgical side of the patient's body faced the ceiling, and the healthy side was placed on the surgical bed in a hybrid OR. As the dosimeters covered the healthy side of the chest from the start of general anaesthesia to the end of surgery, all dosimeters could measure the patient's skin radiation exposure using a CBCT scan in a hybrid OR. Each device recorded not only the exposure dose but also information on the location of the dosimeter and number of CBCT scans. Radiology technicians manually adjusted the field of view (FOV) in each case because the location of pulmonary lesions differed depending on the case, and radiation dose metrics from fluoroscopy and CBCT, reference cumulative Air Kerma was obtained.

Measurement and simulation in a phantom

To determine the amount of radiation exposed to the patient's entire chest, a fast dose estimation system for interventional radiology (FDEIR)—a Monte Carlo dose estimation system for photons in the diagnostic energy range—was adopted as the dose calculation method in this study [28]. Five wearable dosimeters were attached to five locations—similar to the those for measurements in the patients—on a Chest phantom PBU-SS-2® (Kyoto Science, Kyoto, Japan) for obtaining demo data for each shot from 1 to 5 times (Fig. 3). As described in our previous report, FDEIR calculated the absorbed dose to the skin of the chest phantom using FUJITSU Supercomputer PRIMEHPC FX1000 and FUJITSU Server PRIMERGY GX2570 (Wisteria/BDEC-01; FUJITSU Corp., Japan) at the Information Technology Center of the University of Tokyo [28].

Statistical analysis

Descriptive statistics and categorical variables were computed using standard formulae in Excel 2019 ver. 16.0.12527.20260® (Microsoft Corp, Tokyo, Japan) and SPSS Statistics® version 27 (IBM Corp., Armonk, NY, USA). Scatter plots and correlation coefficient analyses were performed using the statistical software R version 4.2.3 (R Foundation for Statistical Computing, Vienna,

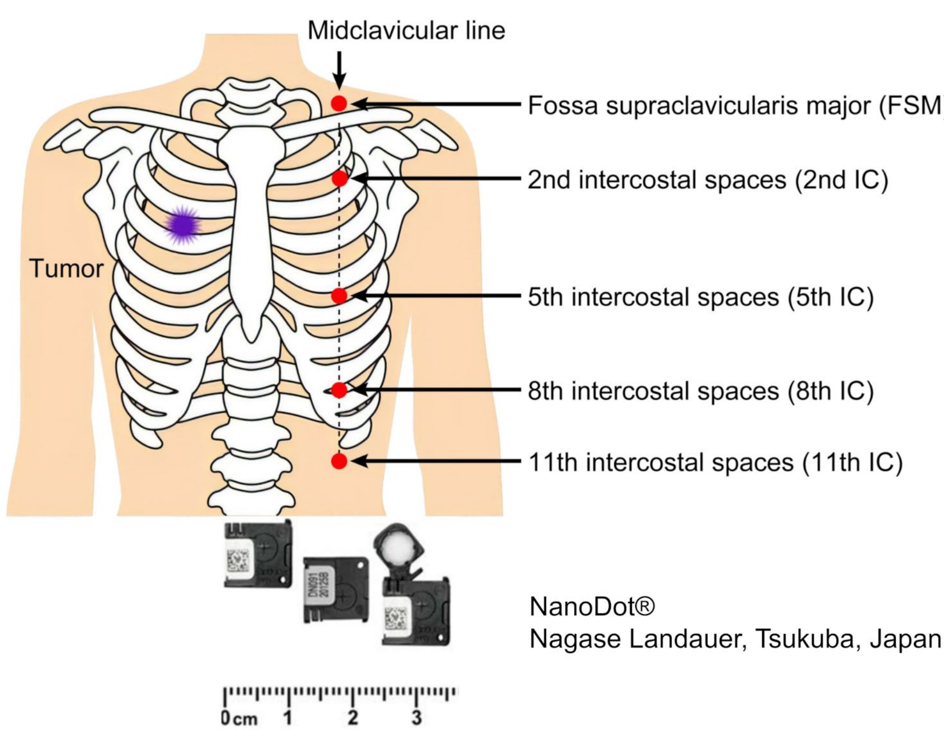

Fig. 2 Five wearable dosimeters are placed on patients' bodies in a hybrid operating room. These dosimeters are attached to the middle axillary line opposite the target. Each dosimeter is located on the fossa supraclavicularis major (FSM), 2nd intercostal space, 5th intercostal space (5th IC), 8th intercostal space (8th IC), or 11th intercostal space (11th IC)

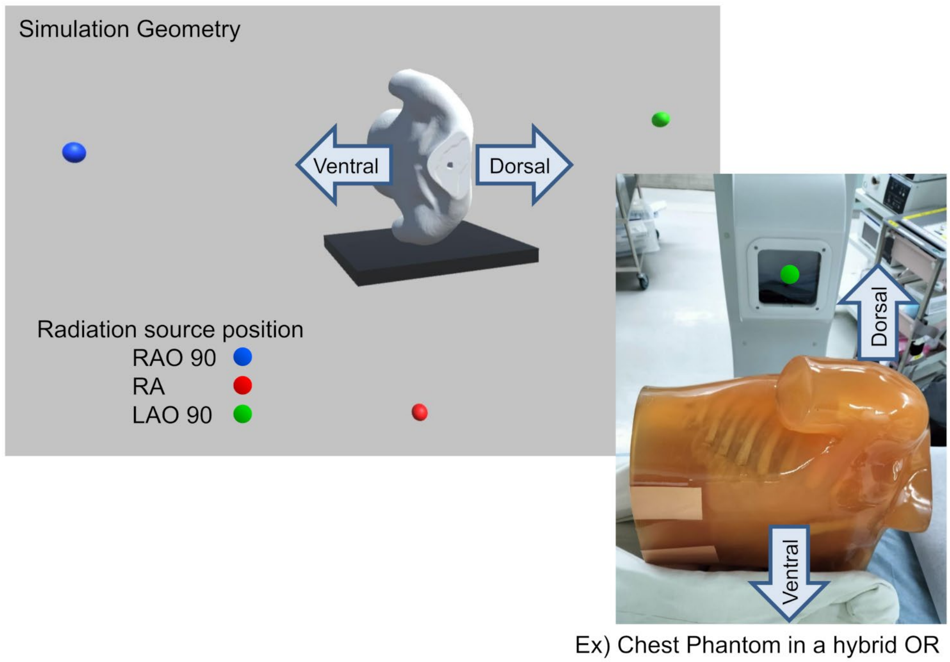

Fig. 3 Phantom experiments was conducted using five wearable dosimeters for measurement of skin radiation dose of a Chest phantom PBU-SS-2® (Kyoto Science, Kyoto, Japan), a table, and air for simply resembling a hybrid operating room suite. And this system was used as a reference for the Monte Carlo simulation

Austria) with the ggplot2 package. A *P*-value < 0.05 was deemed statistically significant.

Ethical considerations

It was necessary to notify or disclose information to all patients in this study about the purpose of the research, and to guarantee the opportunity to refuse as much as possible.

Results

Patient characteristics

Patient characteristics are shown in Table 1. In total, 1,014 surgeries were performed at our institute, including 182 surgeries performed in a hybrid OR between April 2019 and December 2023 (Fig. 1). Among them, 67 patients had data on radiation exposure suitable for analysis and were therefore included in our study. The patients' mean age was 60.7 (29–81) years, and there were 42 males (62.7%) and 25 females (37.3%). Average body mass index (BMI) was 24.3 (18.5–41.4). Most cases were single lesions, and the surgical procedure was thoracoscopic single-wedge resection in approximately 70% of cases. The average number of CBCT scans was 2.1 (1–5), and the identification rate was 100%. No complications related to intraoperative localization were observed. The mean value of patients' radiation exposure was 9.0 mGy per scan. Average radiation dose increased in proportion to Cumulative Air Kerma when all scan times were 1, 2, and 3times. Meanwhile, it increased in proportion to BMI only when scan times 2 or 3 times.

Characteristics of nodules

Surgery was performed on the right side in 41 (62.7%) and left side in 26 (38.8%) patients. Table 2 shows the locations of 78 lesions: 40 in the upper lobe (51.3%), 5 in the middle lobe (6.4%), and 33 in the lower lobe (42.3%). CBCT imaging was carefully limited if the pulmonary lesion was located in the lung apex or above the diaphragm because the C-arm may collide with patient's arm, the anesthesia machine and/or operating table. As a result of operating the CBCT to avoid hitting such an obstacle, the center of FOV was far away from the target lesion, especially in the upper and lower lobe lesions. The average tumour size was 11.8 (2–40) mm on MDCT, 11.3 (2–40) mm on CBCT, and 13.8 (3–80) mm in pathological examination. Consolidation/Tumour ratio (C/T ratio) demonstrated 47 solid nodules (61.8%), 17 subsolid nodules (22.4%), and 12 pure ground-glass nodules (15.8%). Pathological examination revealed 31 primary lung cancers (39.7%), 31 metastatic tumours (39.7%), 4 infectious diseases (5.1%), 2 fibroses (2.6%), 2 benign tumours (2.6%), and 8 other diseases (12.8%). The detection rate of target lesions was 100% in the hybrid OR, and no marking-related complications were confirmed.

Table 1 Clinical characteristics of study patients ($N=67$). Characteristics of patients who were enrolled into this study. Most patients were male who had single pulmonary lesions on right side chest. Wedge resection accounted for the majority, and no marking-related complications were observed. Average number of scan times of cone-beam computed tomography was 2.1 ± 0.79, and average radiation exposure (per scan) was 9.0 ± 5.57 mGy

Characteristic	*n* (%)
Age, years	60.7 ± 14.0
Sex	
Male	42 (62.7)
Female	25 (37.3)
BMI	24.3 ± 3.74
Side	
Right	41 (61.2)
Left	26 (38.8)
Number of pulmonary lesions	
Single	53 (79.1)
Double	8 (11.9)
Triple	3 (4.5)
Multiple	3 (4.5)
Surgical procedure	
Single-wedge resection	48 (71.6)
Bi-wedge resection	9 (13.4)
Segmentectomy	3 (4.5%)
Lobectomy	2 (3.0)
Other	5 (7.5%)
Intraoperative adhesions	12 (17.9)
Time (surgery, min)	130.7 ± 66.2
Time (anaesthesia, min)	211.3 ± 71.6
Blood loss (mL)	29.7 ± 92.6
Complication	0 (0)
Number of scan times	2.1 ± 0.79
Cumulative Air Kerma (mGy)	25.4 ± 19.3
Radiation exposure (mGy per scan)	9.0 ± 5.57

Data on age, time, blood loss, and radiation exposure are presented as mean ± SD

Table 2 Characteristics of pulmonary nodules ($N=78$). Characteristics of pulmonary nodules in this study. Most lesions were located in the upper or lower lobes. Average tumor size was 11.8 ± 6.6, 11.3 ± 7.2, and 13.8 ± 11.5 on MDCT, CBCT, and pathology, respectively. Most lesions were solid nodules on the images, and primary lung cancer and metastatic tumors each accounted for about 40%. The detection rate by CBCT was 100%

Characteristic	*n* (%)
Lobe	
Upper	40 (51.3)
Middle	5 (6.4)
Lower	33 (42.3)
Tumour Size on MDCT (mm)	11.8 ± 6.6
Tumour Size on CBCT (mm)	11.3 ± 7.2
Tumour Size on pathology (mm)	13.8 ± 11.5
Consolidation/Tumour Ratio on MDCT	
Solid (1)	47 (61.8)
Sub-solid (0<, < 1)	17 (22.4)
Pure ground glass opacity (0)	12 (15.8)
Pathological diagnosis	
Lung cancer	31 (39.7)
Metastatic tumours	31 (39.7)
Infectious diseases	4 (5.1)
Pulmonary fibrosis	2 (2.6)
Benign tumour	2 (2.6)
Other	8 (12.8)
CBCT detection rate	78 (100)

Data on tumor size are presented as mean ± SD

CBCT; cone-beam computed tomography, MDCT; multi-detector computed tomography

Skin radiation dose

The row data for the radiation values and scan times are summarised in Supplementary Table 1, where each value was expressed in milligray (mGy). Average skin radiation dose was 1.53, 3.59, 7.14, 5.04, and 1.20 mGy at FSM, 2nd-IC, 5th-IC, 8th-IC, and 11th-IC, respectively. In this study, patient's radiation exposure dose demonstrated a proportional relationship with Air Kerma for all CBCT scans, meanwhile it showed no proportional relationship with BMI at single CBCT scan (Fig. 4). In Fig. 5, the location with the highest radiation exposure was the 5th IC, whereas the locations with the lowest exposure were FSM and 11th IC. Although the doses increased in proportion to the number of scans, it was observed that two locations, the 5th and 8th IC were significantly affected by CBCT irradiation. On the other hand, the exposure dose was found to be less at the FSM and 11th IC. Similarly, higher radiation exposure was measured at 5th and 8th IC in a phantom experiments, however the measured values were higher in the patient than in the phantom. In addition, it was also suggested that the patient's exposure dose may increase if the number of imaging was four or more.

Radiation dose of a phantom

The Monte Carlo method was adopted to visualise radiation exposure to the entire chest of the phantom (Fig. 6). The image was generated with computer simulation as described in detail in our previous report [28]. The bar on the right, displayed on a logarithmic scale where the maximum value was one, shows relative radiation exposure dose by color.The image indicated that the surgical side was also exposed to radiation by CBCT, similar to the non-surgical side attached to the five dosimeters.

Discussion

In this study, intraoperative localization was performed in 182 patients in a hybrid OR during the study period, and radiation exposure was measured in 67 patients. As published in our previous paper, no needle and/or bronchoscopy was required preoperatively for the localization of pulmonary target lesions, which could be identified by intraoperative CT alone [26].

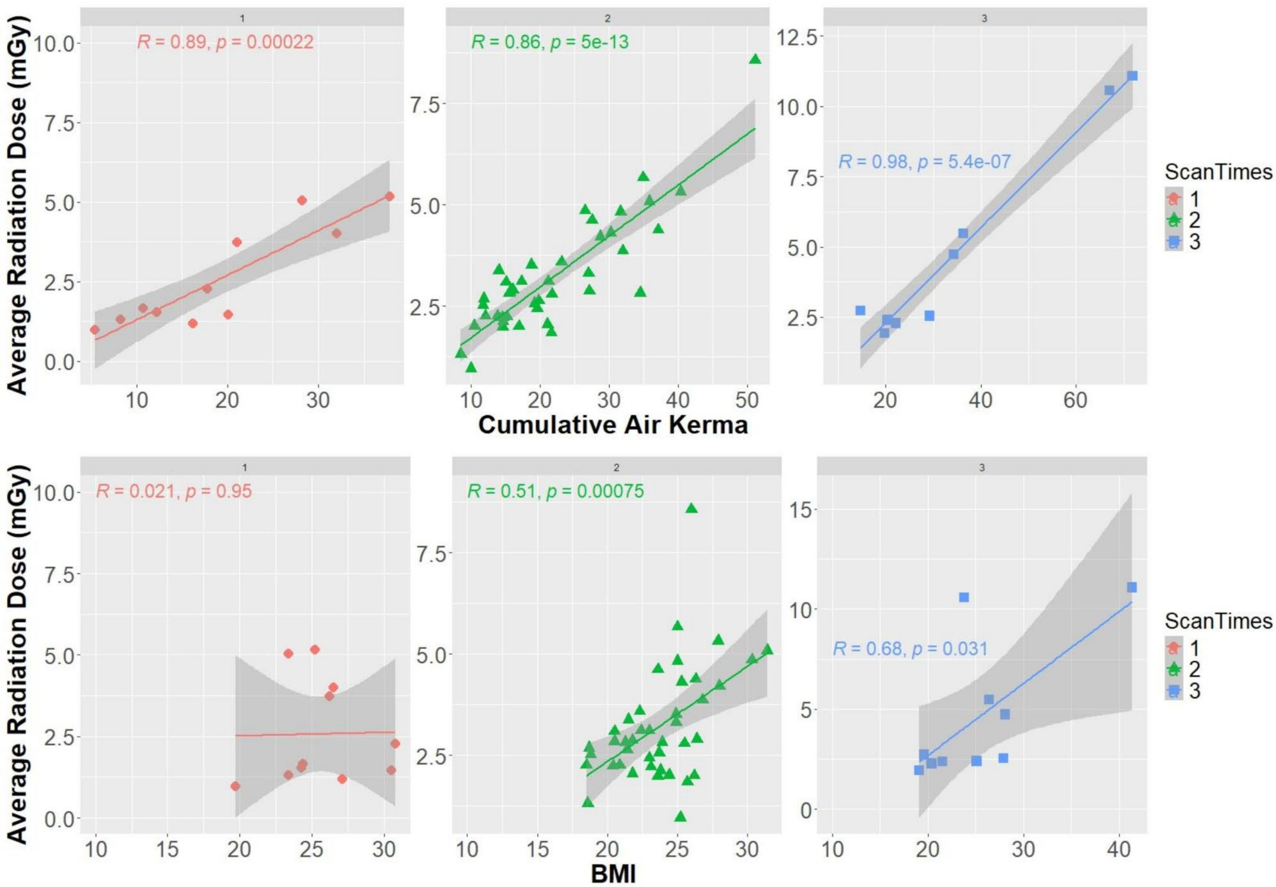

Fig. 4 Patient's radiation exposure dose related with cumulative Air Kerma and body mass index (BMI). Please note that this figure excluded some cases with 4 and 5 scan times because of small case number. As Air Kerma increases, patient radiation exposure dose increases. Similarly, as BMI increased, the patient's radiation exposure dose increased, but an exception was observed in the group of patients with single scan time

Using our identification method, the average number of CBCT scans was 2.1 (1–5), and the detection rate was 100%, with no marking-related complications. Therefore, we believe that the final challenge with this method is to control and reduce radiation exposure in patients.

In 2008, Kan et al. performed a comprehensive study on organ absorbed doses from CBCT demonstrating that the mean skin dose to chest was 64 mGy which was higher than 9.0 mGy per scan in our study [29]. Most other previous studies measured radiation exposure in patients or healthcare workers during radiology or dental examinations. Hsieh et al. used C-arm in a hybrid OR for identification of small solitary pulmonary nodules, reporting the median radiation exposure was 223.2 mGy (Exam Protocol' of the ARTIS zeego instrument) [27]. The value was an excerpt of the structured report on the X-ray radiation dose, so it is impossible to compare with our data. Referring to our cumulative Air-Kerma data (25.4 mGy), radiation exposure dose in their method may result in higher than that in our method. In Fig. 4, patient's radiation exposure dose increased positively as cumulative Air Kerma increased, but it was not uniform from FSM to 11th IC in Fig. 5. Thus, although there are a few reports on estimated values of radiation exposure dose provided by CBCT device, there has been no research about radiation exposure measurement during chest surgeries by attaching the measurement device directly to patients.

In literature, the Monte Carlo simulation was used to calculate the absorbed radiation dose in a set of organs and tissues, including skin (0.06–0.09 mGy) [30]. In our data, the average value of a phantom was 1.89 mGy per CBCT scan. However, it was impossible to simply compare because Maria et al. aimed to measure the exposure dose to internal organs, whereas we measured the skin dose. Furthermore, direct comparisons must be difficult because BMI differs between phantom and actual measurements for each patient. In 2018, Takata et al. reported the usefulness of a fast skin dose estimation system for interventional radiology, which calculates the patient skin dose [28]. In this study, the Monte Carlo method was adjusted to

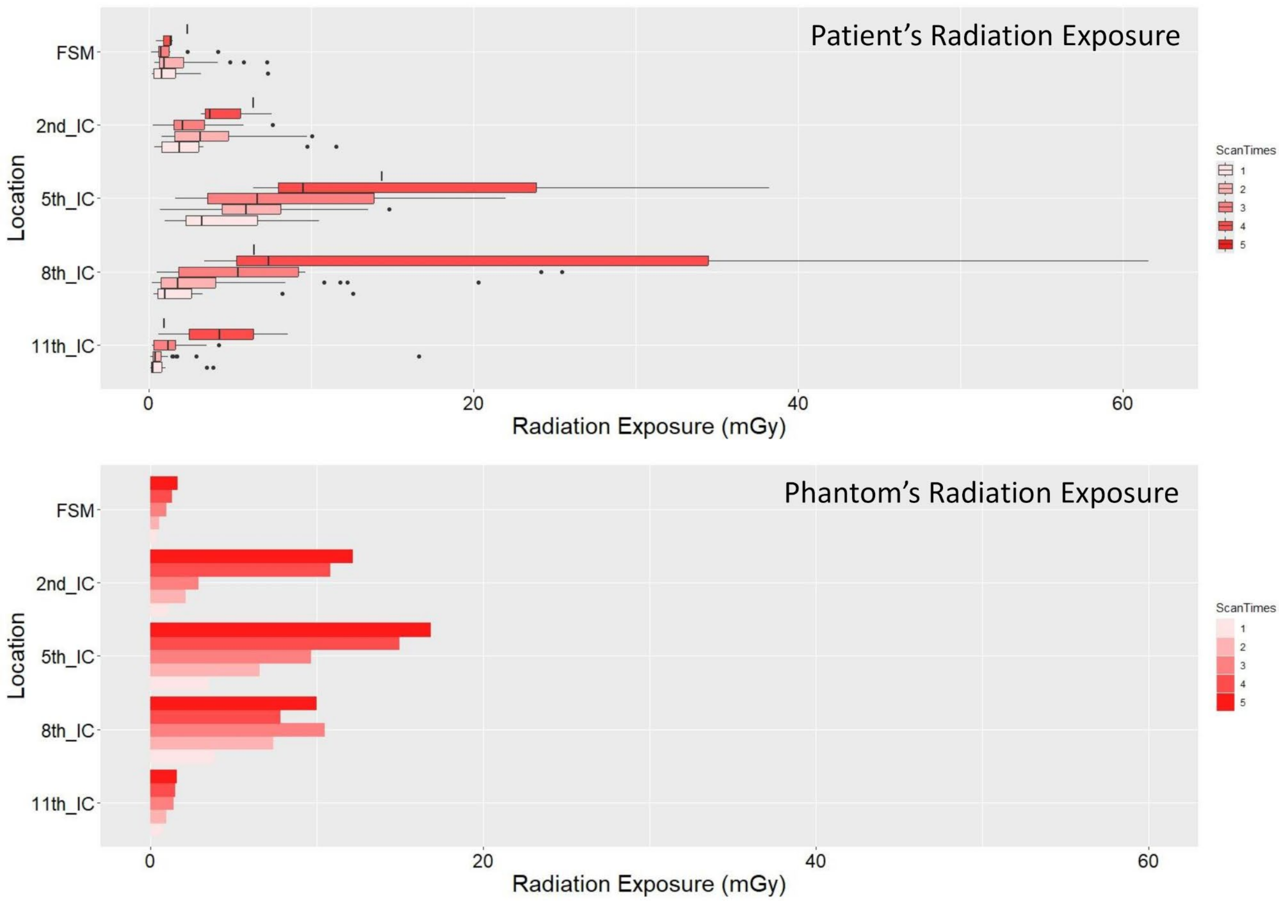

Fig. 5 Boxplots and dot plots demonstrate the patients' and phantoms' radiation exposure doses (mGy). The X-axis shows the scaled radiation exposure (mGy), and the Y-axis shows the location of the wearable dosimeters. Each box demonstrates an interquartile range with a 25% percentile, median, and 75% percentile in patient's radiation exposure. The colour of each box indicates the scan time from pink to red

simulate the skin radiation dose on the surgical side, for which direct measurement is usually not possible because the surgical field must be kept clean to prevent surgical site infections. The Monte Carlo method displayed the distribution of the exposure dose based on the phantom data in Fig. 6, showing that the surgical side was also highly exposed to radiation by CBCT in two locations (5th and 8th IC). This finding indicates that, in many cases, these two locations are included in the irradiation field. In the surgical field, it was technically difficult to position the FSM and 2nd IC at the center of the FOV because the patient's arm and anesthesia machine interfered with the C-arm of CBCT. Similarly, it was difficult to position 11th IC in the center of the FOV because the surgical board on which the surgical instruments were placed interfered with it. As a result, there were many cases in which the center of the FOV was located near the remaining 5th and 8th ICs, and it was considered that the radiation exposure dose in these areas was greater than in other locations. In this study, it was proven that the radiation exposure dose was largely biased in the 5th to 8th IC range, so it would be better to use data from these two sites when comparing to other methods in the near future. In addition, it was also found that reducing the radiation exposure dose to these areas would be effective for patients with general thoracic surgery.

Regarding the comparison between phantom data and actual measurements, the following findings were obtained. (1) the measured values were almost the same as the phantom data at two locations (FSM and 11th IC), but slight differences were observed at the remining locations (2nd, 5th, 8th IC), (2) the measured values were almost the same as the phantom data when CBCT scan 1 to times, but large differences were observed if the number of CBCT scan times was 4 or more. It was speculated that these findings were caused by the factor that the CBCT center was restricted to the area from 5th to 8th during thoracic surgery. While the phantom doll in this study had no arms, the actual patients had arms, so the difference in radiation exposure dose at the 2nd IC may have been observed. It was unclear why the actual radiation exposure dose increased as the number of scan times

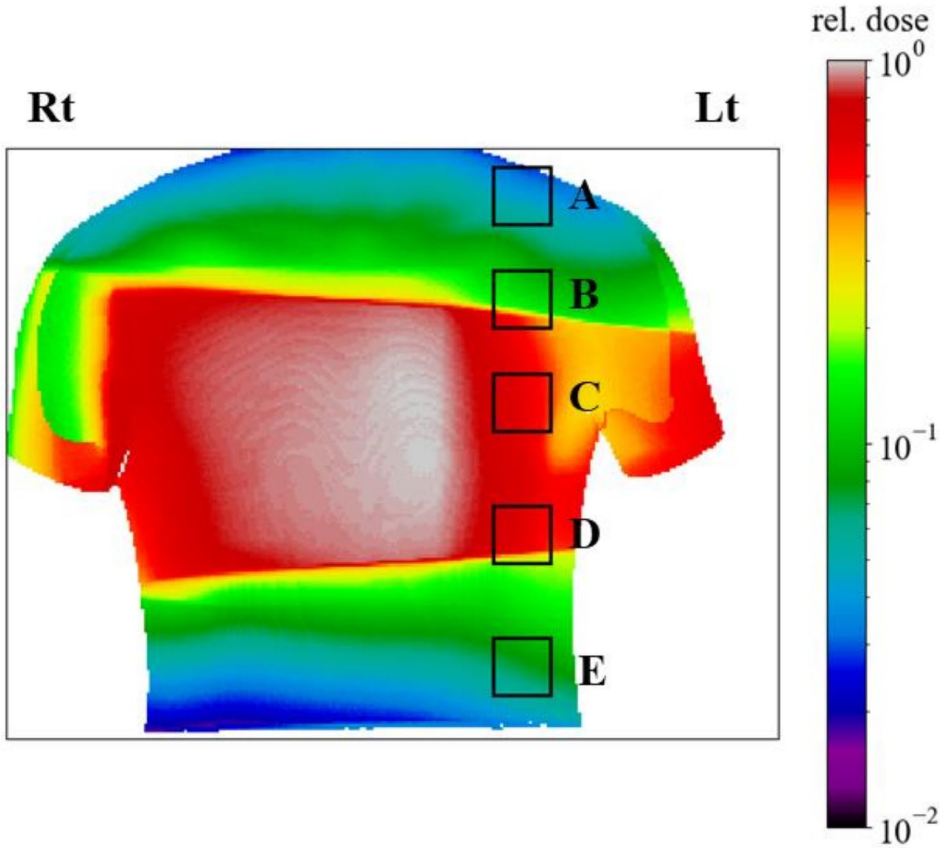

Fig. 6 Images were generated using the Monte Carlo method as described in detail in our previous report. The bar on the right, displayed on a logarithmic scale where the maximum value was one, shows the relative radiation exposure dose by colour. Radiation exposure is mainly concentrated in three central areas (**B**, **C**, and **D**); in contrast, the low dose area is observed in the upper and lower area (**A** and **E**). **A**, **B**, **C**, **D**, and **E** are the fossa supraclavicularis major and the 2nd, 5th, 8th, and 11th intercostal spaces, respectively

increased near the center of CBCT. However, we have learned that it would be better to limit the number of scan times to 3 or less. The difference in the number of scan 4 or more times is a topic for future research.

Limitations

This study had several limitations. It had a relatively small number of cases and was a single institutional study. Next, we only conducted the patient's skin radiation exposure dose in this study, i.e. no data was obtained about radiation exposure of internal tissues inside and outside FOV. Currently, there are various intraoperative identification methods, and there are no medical institutes using the same method as ours; therefore, it is difficult to conduct multicentre joint research to collect more cases. Nevertheless, we believe that it is important to compare patients' radiation exposure among different intraoperative identification methods, and a multicentre prospective study is currently underway.

Conclusions

In conclusion, the patient's 5th to 8th IC was the most radiation exposed area by intraoperative CBCT imaging during thoracic surgery because of the limitation of CBCT motion interference with the patient arm and various equipment related to surgery. In future, it is strongly required to research for radiation protection in this area, and it is also necessary to make efforts to limit the number of scans to three or less, in order to avoid occasional extremely large radiation exposure.

Abbreviations

CBCT	Cone-beam computed tomography
CT	Computed tomography
OR	Operating room
EVAR	Endovascular aortic repair
TAVI	Transcatheter aortic valve implantation
MDCT	Multi-detector computed tomography
FSM	Fossa supraclavicularis major
IC	Intercostal midclavicular line
FDEIR	Fast dose estimation system for interventional radiology

Supplementary Information

The online version contains supplementary material available at https://doi.org/10.1186/s13019-024-03182-z.

Supplementary Material 1

Supplementary Material 2

Acknowledgements

The authors would like to thank Mr. Yusuke Abe, Mr. Kuniaki Shimizu, Mr. Takayuki Yamashita, Mr. Seishin Sasaki, and Mr. Takahiro Futai for providing excellent technical assistance. And, we would like to thank Honyaku Center Inc. for English language editing.

Author contributions

SK, YSai, SM, RT, TK, TN, and HD measured radiation exposure of patients by wearable dosimetry, and IK acquisition of data from each dosimetry. TT simulated radiation exposure of a phantom by a Monte Carlo dose estimation system. SK and YSai analysed the data, and YSai wrote the manuscript. YSai designed the study, and performed the statistical analysis. YY, MK, and YSak provided critical feedback. All authors read and approved the final manuscript.

Funding

Not applicable.

Data availability

No datasets were generated or analysed during the current study.

Declarations

Ethics approval and consent to participate

This study was approved by Teikyo University Medical Research Ethics Committee.

Consent for publication

Not applicable.

Competing interests

The authors declare no competing interests.

Author details

[1]Department of Surgery, Teikyo University School of Medicine, 2-11-1 Kaga, Itabashi-ku, Tokyo 173-8605, Japan
[2]Advanced Comprehensive Research Organization, Teikyo University, Tokyo, Japan
[3]Research Institute of Nuclear Engineering, University of Fukui, Fukui, Japan
[4]Teikyo University Shinjuku Clinic, Tokyo, Japan

Received: 7 July 2024 / Accepted: 1 December 2024
Published online: 19 December 2024

References

1. Sung H, Ferlay J, Siegel RL, Laversanne M, Soerjomataram I, Jemal A, Bray F. Global Cancer statistics 2020: GLOBOCAN estimates of incidence and mortality worldwide for 36 cancers in 185 countries. CA Cancer J Clin. 2021;71:209–49.
2. National Lung Screening Trial Research Team, Aberle DR, Adams AM, Berg CD, Black WC, Clapp JD, Fagerstrom RM, Gareen IF, Gatsonis C, Marcus PM, Sicks JD. Reduced lung cancer mortality. N Engl J Med. 2011;365:395–409.
3. de Koning HJ, van der Aalst CM, de Jong PA, Scholten ET, Nackaerts K, Heuvelmans MA, Lammers JJ, Weenink C, Yousaf-Khan U, Horeweg N, van 't Westeinde S, Prokop M, Mali WP, Mohamed Hoesein FAA, van Ooijen PMA, Aerts JGJV, den Bakker MA, Thunnissen E, Verschakelen J, Vliegenthart R, Walter JE, Ten Haaf K, Groen HJM, Oudkerk M. Reduced lung-cancer mortality with volume CT screening in a randomized trial. N Engl J Med. 2020;382:503–13.
4. Postmus PE, Kerr KM, Oudkerk M, Senan S, Waller DA, Vansteenkiste J, Escriu C, Peters S, ESMO Guidelines Committee. Early and locally advanced non-small cell lung cancer (NSCLC): ESMO Clinical Practice guidelines for diagnosis, treatment, and follow-up. Ann Oncol. 2017;28:iv1–21.
5. NCCN Clinical Practice Guidelines in Oncology (NCCN Guidelines®). Non-Small Cell Lung Cancer Version 1. https://www.nccn.org/guidelines/guidelines-detail?category=1&id=1450. December 2023; Accessed 3 January 2024.
6. Altorki NK, Wang X, Wigle D, Gu L, Darling G, Ashrafi AS, Landrenau R, Miller D, Liberman M, Jones DR, Keenan R, Conti M, Wright G, Veit LJ, Ramalingam SS, Kamel M, Pass HI, Mitchell JD, Stinchcombe T, Vokes E, Kohman LJ. Perioperative mortality and morbidity after sublobar versus lobar resection for early stage NSCLC: Post hoc analysis of an international, randomised, phase 3 trial (CALGB/Alliance 140503). Lancet Respir Med. 2018;6:915–24.
7. Committee for Scientific Affairs, The Japanese Association for Thoracic Surgery, Shimizu H, Okada M, Toh Y, Doki Y, Endo S, Fukuda H, Hirata Y, Iwata H, Kobayashi J, Kumamaru H, Miyata H, Motomura N, Natsugoe S, Ozawa S, Saiki Y, Saito A, Saji H, Sato Y, Taketani T, Tanemoto K, Tangoku A, Tatsuishi W, Tsukihara H, Watanabe M, Yamamoto H, Minatoya K, Yokoi K, Okita Y, Tsuchida M, Sawa Y. (2021) Thoracic and cardiovascular surgeries in Japan during 2018: Annual report by the Japanese Association for Thoracic Surgery. Gen Thorac Cardiovasc Surg 69:179–212.
8. Plunkett MB, Peterson MS, Landreneau RJ, Ferson PF, Posner MC. Peripheral pulmonary nodules: preoperative percutaneous needle localization with CT guidance. Radiology. 1992;85:274–6.
9. Mack MJ, Gordon MJ, Postma TW, Berger MS, Aronoff RJ, Acuff TE, Ryan WH. Percutaneous localization of pulmonary nodules during thoracoscopic lung resection. Ann Thorac Surg. 1992;53:1123–4.
10. Sakiyama S, Kondo K, Matsuoka H, Yoshida M, Miyoshi T, Yoshida S, Monden Y. Fatal air embolism during computed tomography-guided pulmonary marking with a hook-type marker. J Thorac Cardiovasc Surg. 2003;126:1207–9.
11. Horan TA, Pinheiro PM, Araújo LM, Santiago FF, Rodrigues MR. Massive gas embolism during pulmonary nodule hook-wire localization. Ann Thorac Surg. 2002;73:1647–9.
12. Kerrigan DC, Spence PA, Crittenden MD, Tripp MD. Methylene blue guidance for the simplified resection of lung lesions. Ann Thorac Surg. 1992;53:163–4.
13. Wicky S, Mayor B, Cuttat JF, Schnyder P. CT-guided localization of pulmonary nodules with methylene blue injections for thoracoscopic resection. Chest. 1994;106:1326–8.
14. Hasegawa T, Kuroda H, Sato Y, Matsuo K, Sakata S, Yashiro H, Sakakura N, Mizuno T, Arimura T, Yamaura H, Murata S, Imai Y, Sakao Y, Inaba Y. Utility of indigo carmine and lipiodol mixture for preoperative pulmonary nodule localization before video-assisted thoracic surgery. J Vasc Interv Radiol. 2019;30:446–52.
15. Nomori H, Horio H. Coloured collagen is a long-lasting point marker for small pulmonary nodules in thoracoscopic operations. Ann Thorac Surg. 1996;61:1070–3.
16. Kobayashi T, Kaneko M, Kondo H, Nakayama H, Asamura H, Tsuchiya R, Naruke T, Kakizoe T. CT-guided bronchoscopic barium marking for resection of a fluoroscopically invisible peripheral pulmonary lesion. Jpn J Clin Oncol. 1997;27:204–5.
17. Asano F, Shindoh J, Shigemitsu K, Miya K, Abe T, Horiba M, Ishihara Y. Ultrathin bronchoscopic barium marking with virtual bronchoscopic navigation for fluoroscopy-assisted thoracoscopic surgery. Chest. 2004;126:1687–93.
18. Sato M, Omasa M, Chen F, Sato T, Sonobe M, Bando T, Date H. Use of virtual assisted lung mapping (VAL-MAP), a bronchoscopic multispot dye-marking technique using virtual images, for precise navigation of thoracoscopic sublobar lung resection. J Thorac Cardiovasc Surg. 2014;147:1813–9.
19. Nagano M, Sato M. (2023) Ten-year outcomes and development of virtual-assisted lung mapping in thoracic surgery. Cancer (Baseline) 15:1971.
20. Upchurch GR Jr, Escobar GA, Azizzadeh A, Beck AW, Conrad MF, Matsumura JS, Murad MH, Perry RJ, Singh MJ, Veeraswamy RK, Wang GJ. Society for Vascular Surgery Clinical Practice guidelines for thoracic endovascular aortic repair for descending thoracic aortic aneurysms. J Vasc Surg. 2021;73(1S):S55–83.
21. Debono S, Nash J, Tambyraja AL, Newby DE, Forsythe RO. Endovascular repair for abdominal aortic aneurysms. Heart. 2021;107:1783–9.
22. Sundt TM, Jneid H. Guidelines update on indications for transcatheter aortic valve implantation based on the 2020 American College of Cardiology/American Heart Association Guidelines for Management of Valvular Heart Disease. JAMA Cardiol. 2021;6:1088–9.
23. Lee G, Chikwe J, Milojevic M, Wijeysundera HC, Biondi-Zoccai G, Flather M, Gaudino MFL, Fremes SE, Tam DY. ESC/EACTS vs. ACC/AHA guidelines for the management of severe aortic stenosis. Eur Heart J. 2023;44:796–812.

24. Zhang G, Xu D, Yu Z, Wang L, Gu H, Chai Y, Shen G. Preoperative non-invasive visual localization of synchronous multiple lung cancers using three-dimensional computed tomography lung reconstruction. J Cardiothorac Surg. 2021;6:273.
25. Sekimura A, Iwai S, Yamagata A, Motono N, Usuda K, Uramoto H. Virtual thoracoscopic imaging-assisted pleural marking of pulmonary nodules. J Thorac Dis. 2020;12:4148–56.
26. Saito Y, Watanabe T, Kanamoto Y, Asami M, Yokote F, Dejima H, Morooka H, Ibi T, Yamauchi Y, Takahashi N, Ikeya T, Sakao Y, Kawamura M. Pilot study of intraoperative localization of peripheral small pulmonary tumours using cone-beam computed tomography: a sandwich marking technique. J Thorac Dis. 2022;14:2845–54.
27. Hsieh MJ, Fang HY, Lin CC, Wen CT, Chen HW, Chao YK. Single-stage localization and removal of small lung nodules through image-guided video-assisted thoracoscopic surgery. Eur J Cardiothorac Surg. 2018;53:353–8.
28. Takata T, Kotoku J, Maejima H, Kumagai S, Arai N, Kobayashi T, Shiraishi K, Yamamoto M, Kondo H, Furui S. Fast skin dose estimation system for interventional radiology. J Radiat Res. 2018;59:233–9.
29. Kan MW, Leung LH, Wong W, Lam N. Radiation dose from cone beam computed tomography for image-guided radiation therapy. Int J Radiat Oncol Biol Phys. 2008;1:70:272–9.
30. Maria R, Soares WS, Santos LP, Neves, Ana P, Perini, Wilson OG, Batista W, Belinato AF, Maia, Linda VE, Caldas. Dose estimate for cone beam CT equipment protocols using Monte Carlo simulation in computational adult anthropomorphic phantoms. Radiat Phys Chem. 2019;155:252–9.

Publisher's note